Received: 4 January 2023 | Revised: 15 January 2023 | Accepted: 12 February 2023

DOI: 10.1002/pc.27285

RESEARCH ARTICLE

Polymer COMPOSITES WILEY

Optimization of Charpy-impact strength of 3D-printed carbon fiber/polyamide composites by Taguchi method

Bertan Beylergil[1] | **Abdulrahman Al-Nadhari**[2] | **Mehmet Yildiz**[2,3]

[1]Faculty of Engineering, Department of Mechanical Engineering, Alanya Alaaddin Keykubat University, Alanya, Turkey

[2]Faculty of Engineering and Natural Sciences, Sabanci University, Istanbul, Turkey

[3]Composite Technologies Center of Excellence, Istanbul Technology Development Zone, Sabanci University-Kordsa, Istanbul, Turkey

Correspondence
Bertan Beylergil, Faculty of Engineering, Department of Mechanical Engineering, Alanya Alaaddin Keykubat University, Alanya, 07450, Turkey.
Email: bertan.beylergil@alanya.edu.tr

Mehmet Yildiz, Faculty of Engineering and Natural Sciences, Sabanci University, Tuzla, Istanbul, 34956, Turkey.
Email: mehmet.yildiz@sabanciuniv.edu

Funding information
The Scientific and Technological Research Council of Turkey, Grant/Award Number: 219M076

Abstract

This study utilizes the Taguchi optimization technique to investigate the effects of FDM processing parameters on the Charpy impact strength of 3D printed CF/PA composites experimentally and statistically. The four 3D printing parameters employed in the experiment are the infill density, raster angle, extruder temperature, and printing speed, which were used to create the experimental plan with the L18 orthogonal array. Signal to noise (S/N) ratios and analysis of variance (ANOVA) were utilized to identify the optimum values and the interactions between the process parameters. SEM and thermography techniques were employed to assess the microstructural and damage status of the CF/PA composite specimens. ANOVA results determined that only three factors–infill density, raster angle, and extruder temperature–had a statistical significance, while printing speed did not. The outcomes demonstrated that the optimal 3D printing parameters are infill density (100%), raster angle (60°), extruder temperature (260°C), infill density (100%), and printing speed (30 mm/s), with the maximum contribution of 54.19% belonging to infill density, and the minimum contribution of 2.84% belonging to printing speed. The optimal combination of these 3D printing parameters yielded a Charpy impact strength of 10.54 kJ/m^2, resulting in an increase of almost 150% compared to the worst-case situation. The Taguchi approach proves to be a proficient technique to boost the Charpy impact strength of 3D-printed CF/PA composites.

KEYWORDS

3D printing, composites, fibers, impact resistance, polyamides, Taguchi method

1 | INTRODUCTION

Additive manufacturing, or 3D printing, is an exciting layer-by-layer manufacturing method with incredible potential. With this technology, complex geometries can be produced faster and at a lower cost than traditional manufacturing processes. In addition, since the shape of the part is given with CAD data, this method offers plenty of design flexibility while minimizing material losses and operation steps–making it a great choice for those seeking an efficient and cost-effective way to manufacture parts.[1] 3D printing is an integral part of Industry 4.0 and has revolutionized the production phase by reducing physical movements. Initially, it was only used in the design stage, but thanks to the revolutionary advancements in 3D printing technology, it has now become the preferred method for producing a finished product. This trend has been adopted by many

industries such as automotive, aviation and space, medicine and electrical electronics in recent years with aerospace being at the forefront of this movement. To ensure quality control standards are met with 3D printing manufacturing methods, The American Society for Testing and Materials International (ASTM) continues to work hard to set these standards.[2,3]

Additive manufacturing methods utilized in industry present several advantages, including ease of use, cost-effectiveness, and a facile supply of raw materials. Of these methods, fused deposition modeling (FDM) is the most widely utilized, owing to its straightforward extrusion process. The FDM process consists of a heated nozzle that melts a plastic filament and deposits it layer by layer, following a predetermined path. This method is incredibly easy to use, cost effective, and provides the user with high-quality results. Additionally, the raw material supply for FDM is readily available, making it a popular choice for many industries.[4–6]

The most common thermoplastics for FDM are acrylonitrile butadiene styrene (ABS), polylactic acid (PLA), polyvinyl alcohol (PVA), polycaprolactone (PCL), and polyamide (PA). Despite this, the mechanical properties of parts manufactured through FDM have been found to be very low in rigidity. This lack of mechanical performance limits the use of FDM products in more widespread applications. To address this issue, reinforcing materials such as short fibers or micron/nano-sized particles can be incorporated into 3D-printed parts to improve their mechanical performance. It has been shown that the short fibers in the polymer are oriented along the printing direction during processing, increasing the rigidity and strength of the material in this direction.[7–12] In the other transverse direction, it has been demonstrated that there is a decrease in the material's properties. This signifies that short fiber reinforced composites demonstrate anisotropic behavior. The fabrication of these materials with FDM has generated a novel area in additive manufacturing. Even though they have reduced mechanical properties compared to continuous fiber reinforced thermoplastic composites, it is a noteworthy benefit that short fiber reinforced thermoplastic composites can be produced efficiently and cost-effectively with existing 3D printers.[13,14] Consequently, the scientific community has become more and more interested in 3D-printing of short fiber reinforced polymers, as its potential applications are becoming increasingly clear.

Regarding the FDM method, there are numerous parameters which influence the end product's performance and production process. Layer height is a measurement taken in the z-direction and denotes the height of each layer. It is associated with production time; higher layer heights result in faster reaching of final product thickness. Printing speed stands for how far an extruder moves within a certain period. Raster angle measures the angle between x-axis of print area and nozzle path, while fill rate specifies how much material is used during printing.[5] Extensive research has been conducted to evaluate the influence of various parameters on the mechanical characteristics of 3D-printed parts. A comprehensive overview of some recent studies can be found below.

Chacón et al.[15] conducted a detailed study to investigate the relationship between printing parameters, such as printing orientation, layer thickness and printing speed, and tensile and bending test performances of PLA material. It was determined that low layer thickness and high printing speed are necessary for ductile behavior. Wang et al.[16] demonstrated that the raster angle has a concrete effect on the fracture mode of PLA material, while printing speed influences its void ratio, and nozzle temperature affects the fluidity of the material. In the study of Raut et al.,[17] a detailed investigation into the mechanical properties of ABS material for various printing orientations was conducted. Sezer et al.[18] demonstrated that the raster angle has a significant impact on the tensile properties of carbon fiber reinforced ABS composites. Ning et al.[19] assessed the effect of different printing parameters on the mechanical properties of carbon fiber reinforced ABS filament and found that factors such as printing pattern, speed, layer thickness, and extrusion temperature also influence mechanical characteristics of fiber reinforced FDM parts. Toro et al.[5] conducted an in-depth study on the effects of various printing parameters on the mechanical performance of carbon fiber reinforced polyamide (CF/PA) composites. Peng et al.[20] also explored similar topics, specifically examining the impact of raster angle and bed temperature on tensile properties and interlayer bonding. More recently, Shanmugam et al.[21] released a comprehensive review article on mechanical and thermal performance of both reinforced and unreinforced FDM printed polymers.

An extensive body of research has been conducted to investigate the effects of 3D printing parameters on the tensile and flexural properties of CF/PA composites. Specifically, the volume of literature is substantial, providing an intricate and comprehensive understanding of the effects that various parameters have on the aforementioned properties. However, assessing the effects of 3D printing parameters on the impact strength of these composites has not been thoroughly explored. Therefore, it is imperative to ascertain the most effective 3D printing parameters to create high-performance CF/PA parts. To

this end, more research needs to be conducted in this area to understand the influence of different 3D-printing process parameters on the impact resistance of CF/PA composites. This study intends to provide an in-depth analysis of this research gap and serve as a foundation for further investigation in the field.

This investigation, which was motivated by the literature review mentioned above, aimed to determine the effects of FDM processing parameters on the Charpy impact strength of CF/PA composites. Experiments and statistical analysis were conducted using the Taguchi L18 orthogonal array to plan the experiment. This experiment considered four distinct 3D printing parameters: raster angle, infill density, extruder temperature, and printing speed. The Signal to Noise (S/N) ratio and analysis of variance (ANOVA) were used to identify optimal levels and interactions between different processing parameters. Additionally, scanning electron microscopy (SEM) and thermography techniques were employed for microstructure and damage state analysis of composite specimens.

2 | EXPERIMENTAL

2.1 | Materials

This study utilized a CF/PA filament produced by eSUN® Company with a standard diameter of 1.75 mm. The short carbon fiber weight content was 20%, and its corresponding volume content was approximately 14%. The diameter of each carbon fiber was measured to be 7–8 microns, with a variance of no more than 0.1 microns. The filaments had a density of 1.24 g/cm^3 and a melt flow index of 11.46 (275°C/5 kg load). Following the manufacturer's recommendation, they were kept in the eSUN® eBOX Lite 3D filament dryer for 12 h at 70°C to remove absorbed moisture. The recommended printing parameters are as follows: Extruder temperature: 240–260°C, Printing speed: 30–80 mm/s, and Bed temperature: 80°C.

2.2 | Preparation of test specimens and Charpy-impact tests

"A" type of notched Charpy test specimens were produced by MY X30 (CCH Technology, Turkey) 3D printer according to ISO 179 standard. Figure 1A depicts the production of carbon fiber/polyamide composites utilizing a 3D printer. The specimens had dimensions of 80 × 10 × 4 mm^3 (length × width × thickness). The device has a printing volume of 300 × 200 × 250 mm^3, and the position accuracy is 15 microns in the x–y axis, and 5 microns in the z-axis. The maximum bed temperature is 100° C. The 3D-printing plane was chosen to be the XY plane, as it maximizes the area of contact between the polymer and the building platform and to avoid any issues of adhesion that would arise in the XZ plane. A hardened steel nozzle was used as it provides slightly better wear-resistance than brass counterparts. To improve adhesion of the polymer to the bed plate, blue masking tape (3 M Scotch Blue 2090 masking tape) was placed over the printing bed. To ensure a strong adhesion between the specimen and build platform, the build plate adhesion type was adjusted to Brim. The brim line count, width, and speed were set to 10, 25 and 10 mm/s respectively. The linear infill pattern was chosen due to its efficient use of materials. The infill line distance and line width were set to 0.4 mm. The wall speed, travel speed, and initial layer speed were set at 10, 120, and 10 mm/s, respectively.

The bed temperature was maintained at a constant 80°C, with the nozzle diameter and layer height set to 0.4 and 0.2 mm, respectively. The cooling fan on the device was turned off as recommended by the filament manufacturer. In this study, four distinct 3D-printing parameters were considered: raster angle, extruder temperature, infill density, and printing speed. The raster angle was precisely determined as the angle measured in a clockwise direction from the y-axis, with 0° being the point of origin and the angle increasing in a clockwise direction as it progresses. Figure 2 shows the linear infill pattern and the angle direction of the raster.

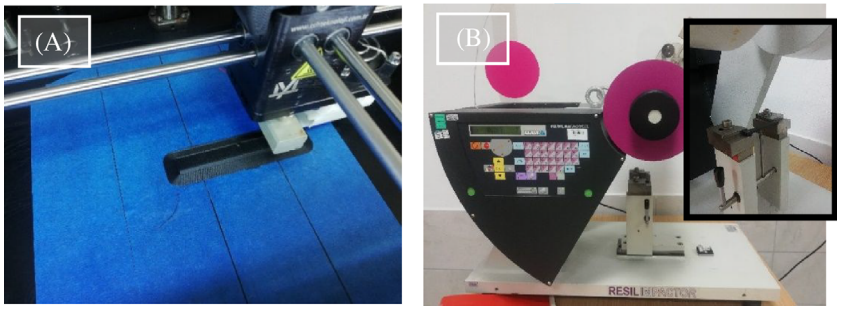

FIGURE 1 (A) Manufacturing of carbon fiber/polyamide composites using the 3D-printer, (B) Charpy test specimen

The levels of each process parameter are provided in Table 1.

The Charpy impact tests were conducted on a minimum of five samples from each group, utilizing a CEAST impact tester (Resil Impactor) with a 4-Joule hammer, in a laboratory environment with a temperature of 24.5°C and relative humidity of 51%. Figure 1B shows of the Charpy impact test specimen prior to impact. During impact testing, the specimen was subjected to a quick and intense blow by a hammer pendulum striking the specimen with a speed of 3.75 m/s. The potential energy difference between the hammer's initial and final positions was used to determine the impact energy. This energy difference was then transformed into Charpy impact strength using the following equation:

$$\text{Charpy impact strength} = \frac{E_a}{b_n.h}\left(\text{kJ/m}^2\right) \quad (1)$$

where b_n and h are the remaining width measured from the notch tip to the free edge and the thickness of the specimen, respectively.

2.3 | Design of experiments

In this study, the Taguchi method was used as the experimental design and analysis method. In this method, a design called OD is used. Each parameter is listed in a column and used to calculate the main effect of the components in the OD. The main effect is a combination of experiments. The appropriate orthogonal array can be chosen by knowing the number of parameters and levels. There are six steps in conducting Taguchi analyses: (1) determining the parameters and levels to be examined, (2) selecting the appropriate orthogonal array, (3) transferring the selected parameters and levels to the columns of the orthogonal array, (4) performing experiments using the orthogonal array, (5) determining signal-to-noise ratios, and (6) performing validation experiments.[22]

The Taguchi method involves finding the solution with the least number of experiments to create better-quality procedures and products.[23] It is well known that the Taguchi method is more efficient than the complete factorial method, which involves using all possible combinations of levels of the variables being tested. Table 1 can be used to find out how many specimen groups are needed, as well as the total number of experiments that need to be conducted in the complete factorial method. A 162 specimen groups would be needed, and 810 test specimens should have been used in total. This would be very time-consuming and expensive to implement. The experimental design for this investigation was carefully constructed using the Taguchi L18 orthogonal array, as shown in Table S1. This method reduced the number of test groups from 162 to 18 and decreased the total amount of test specimens from 810 to 90.

The objective function values are transformed into a signal-to-noise (S/N) ratio using the Taguchi method, which transforms the objective function values into a signal-to-noise (S/N) ratio. The noise represents the variables that were not included in the experimental design but had an impact on the test findings, and the signal represents the actual value received from the system. There are three different S/N ratios depending on how well the outcome fits the situation; (i) "lower is better for the case of minimizing the performance characteristic,", (ii) "nominal better" and (iii) "larger is better". The S/N ratio was chosen as the "larger is better" given by the equation below since this study aims to obtain the highest Charpy impact strength possible.[24]

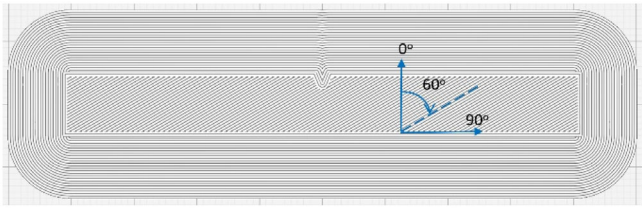

FIGURE 2 The first layer of the composite, raster angle, and linear infill pattern

TABLE 1 3D-printing process parameters and their levels

Level	A-raster angle (°)	B-extruder temperature (°C)	C-printing speed (mm/s)	D-infill density (%)
1	0	240	20	80
2	15	250	30	90
3	30	260	40	100
4	45	—	—	—
5	60	—	—	—
6	75	—	—	—

$$S/N = -10\log\left[\frac{1}{n}\sum_{i=1}^{n}\frac{1}{Y^2}\right] \quad (2)$$

where n and Y is the number of data points the value of the i^{th} data point, respectively. The optimum parameters that offer the best impact resistance are the ones with the highest S/N ratio.

3 | RESULTS AND DISCUSSION

3.1 | Thermal properties of neat PA and CF/PA

The thermal properties of the 3D printed neat PA and CF/PA layers were determined by thermogravimetric analysis (TGA) and differential scanning calorimetry (DSC) techniques. To compare the thermal stability of neat PA and CF/PA filaments, a PA test specimen was printed by using the same printing parameters. All tests were carried out under nitrogen atmosphere with a heating rate of 10°C/min. The thermal analysis system is Mettler Toledo TGA DSC 3 (Columbus, OH). In TGA analysis, the samples were heated from room temperature to 700°C. In DSC analysis, the samples were heated from −100 to 200°C. The TGA curves of the 3D-printed PA and CF/PA layers are shown in Figure 3A. Both PA and CF/PA exhibit a one-step decomposition profile corresponding to polymer pyrolysis. The weight of the samples starts to lose at around 80°C, corresponding to the removal of absorbed water. It was observed that the addition of carbon fiber reduces the amount of moisture. The onset decomposition temperature of neat PA is 383.6°C, and it is increased to 393.7°C for CF/PA with the addition of carbon fibers. The incorporation of carbon fibers improves the thermal stability of the PA matrix. This can be attributed to the physical barrier effect of fibers, which prevents heat from being transferred to the matrix.[25,26]

The mechanical properties of polymers, such as elastic modulus, fracture toughness, yield strength, and heat resistance, are known to be influenced by their crystallinity. Therefore, the melting and crystallization behavior of PA and CF/PA composites were studied using the DSC thermograms shown in Figure 3B. Using the following Equation (3), the degree of crystallinity (X_c) of the specimens was calculated from the DSC thermograms.[27]

$$\text{The degree of crystallinity } (X_c, \%) = \frac{\Delta H_m}{w\Delta H_m^{100\%}} \times 100 \quad (3)$$

where ΔH_m is the measured melting enthalpy of specimen, $\Delta H_m{}^{100\%}$ is the melting enthalpy for 100% crystalline PA, and 'w' is the mass fraction of PA in the composite sample. $\Delta H_m{}^{100\%}$ for the 100% crystalline PA is 206 J/g.[28,29] Table S2 shows the melting and crystallization parameters of PA and CF/PA samples. The presence of carbon fibers increased the crystallinity of PA from 17.4% to 20.2%. This is because the carbon fibers act as heterogeneous nucleation agents for polymer crystallization, and their inclusion also increased the crystallization temperature by 5°C from 147.4 to 152.5°C.

3.2 | Charpy impact test results

The average of the Charpy impact test results for all experimental groups in the DOE are presented in Table 2.

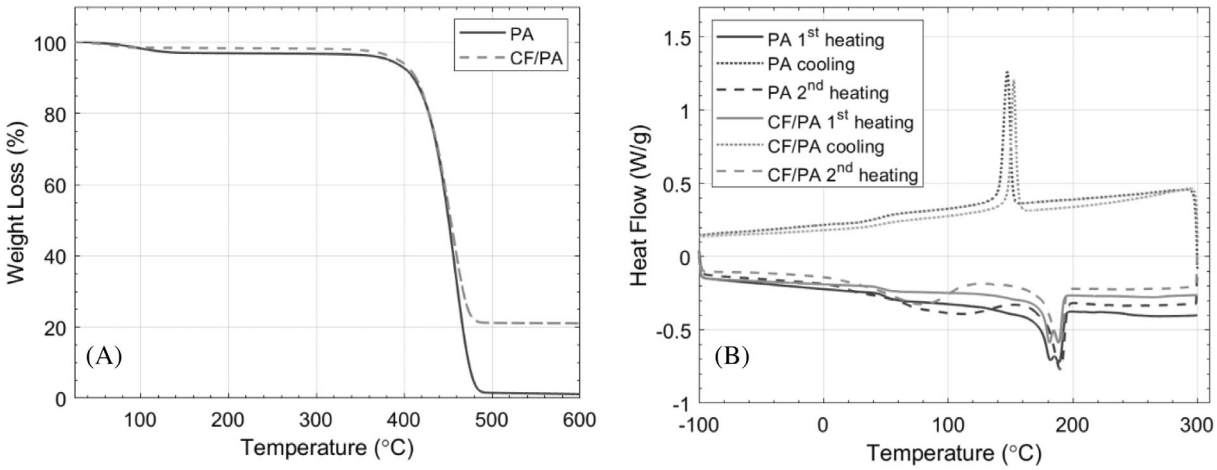

FIGURE 3 (A) Thermogravimetric analysis (TGA) and (B) differential scanning calorimetry (DSC) curves of the polyamide (PA) and carbon fiber/polyamide (CF/PA) 3D-printed layers

TABLE 2 Results of Charpy-impact tests

Group number	A Raster angle (°)	B Extruder temperature (°C)	C Printing speed (mm/s)	D Infill density (%)	Charpy-impact strength (kJ/m^2)	Coefficient of variation (%)
1	1	1	1	1	4.942 ± 0.345	6.9
2	1	2	2	2	6.344 ± 0.241	3.8
3	1	3	3	3	9.525 ± 0.424	4.4
4	2	1	1	2	4.225 ± 0.279	6.6
5	2	2	2	3	9.044 ± 0.471	5.2
6	2	3	3	1	6.556 ± 0.318	4.8
7	3	1	2	1	5.213 ± 0.230	4.4
8	3	2	3	2	4.950 ± 0.135	6.4
9	3	3	1	3	8.950 ± 0.449	5.0
10	4	1	3	3	8.995 ± 0.554	6.1
11	4	2	1	1	6.213 ± 0.151	2.4
12	4	3	2	2	6.775 ± 0.197	2.9
13	5	1	2	3	9.413 ± 0.177	1.9
14	5	2	3	1	7.350 ± 0.362	4.9
15	5	3	1	2	8.766 ± 0.586	6.6
16	6	1	3	2	7.589 ± 0.332	4.4
17	6	2	1	3	8.363 ± 0.204	2.4
18	6	3	2	1	8.331 ± 0.366	4.4

The coefficients of variation for all experimental groups fall within the permitted range for Charpy impact tests, which is 1.9% to 6.9%. The fourth group of the DOE design (DOE-4) has a minimum Charpy impact strength of 4.225 ± 0.279 kJ/m^2. This group is used for comparison in the following subsections and is coded as "A2B1C1D2". The code basically refers to the following 3D printing parameters: Raster angle: 15° (Parameter A-Level 2), Extruder temperature: 240°C (Parameter B -Level 1), Printing speed: 20 mm/s (Parameter C -Level 1) and Infill density: 90% (Parameter D -Level 2). Figure 4A displays the fractured A2B1C1D2 test specimens upon impact loading. The DOE-3 design has the highest Charpy impact strength, which is calculated to be 9.525 ± 0.424 kJ/m^2 (A1B3C3D3). The Charpy impact strength of composites is significantly influenced by the 3D printing parameters. The difference in Charpy impact strength between the lowest and highest values is 125%.

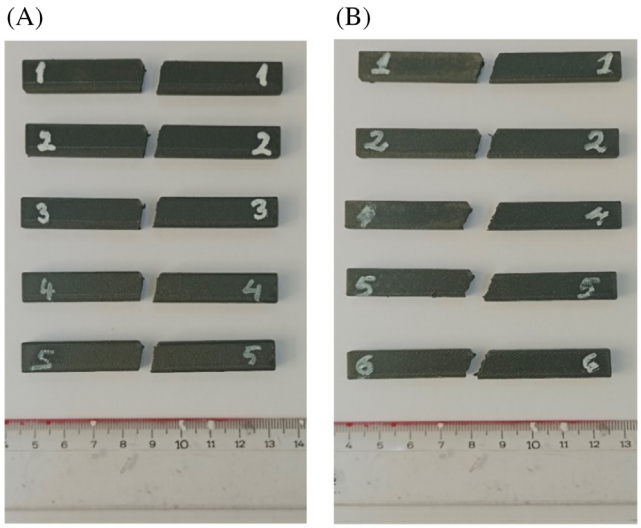

FIGURE 4 (A) A2B1C1D2 (DOE-4) and (B) the optimized specimens (A5B3C2D3) after impact

3.3 | Signal to noise ratios

Table 3 presents the response table for S/N ratios, providing an in-depth analysis on the influence of each parameter on the Charpy impact strength of the CF/PA specimens. It was determined that infill density had the greatest impact (ΔS/N = 3.20 dB), followed by raster angle (ΔS/N = 2.80 dB), extruder temperature (ΔS/N = 1.99 dB), and printing speed had the least influence (ΔS/N = 0.90 dB).

TABLE 3 S/N ratios for Charpy impact strength (Larger is better)

Level	A Raster angle (°)	B Extruder temperature (°C)	C Printing speed (mm/s)	D Infill density (%)
1	16.50	16.15	16.43	16.03
2	15.99	16.78	17.34	15.92
3	15.76	18.14	17.30	19.12
4	17.19	—	—	—
5	18.55	—	—	—
6	18.15	—	—	—
Delta	2.80	1.99	0.90	3.20
Rank	2	3	4	1

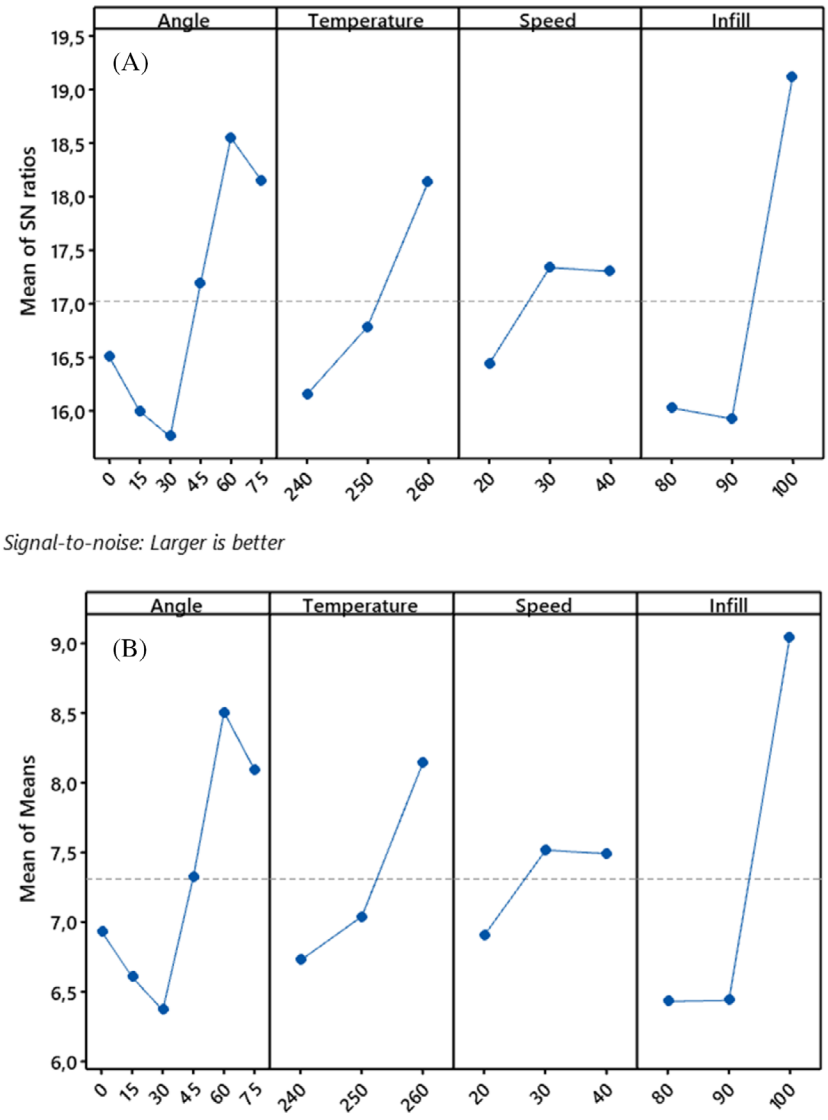

FIGURE 5 Main effects plot for (A) S/N ratios and (B) for means

Figure 5A shows the main effects plots for the S/N ratios. The graph is plotted between the mean of the S/N ratios and the number of levels for all four parameters. The Charpy impact strength increased in proportion to the increase in infill density, due to the additional presence of plastic and carbon fibers within the printed part.

This, in turn, contributed to the enhanced impact strength. Upon examining the printed specimens at different raster angles, it was determined that those printed at a raster angle between 0 and 30° had a lower level of strength and were more brittle than specimens printed at other raster angles. The Charpy impact strength was observed to steadily increase as the raster angle increases, ultimately reaching its peak at 60°. This was further confirmed by SEM observations in the following subsections, which showed that the amount of carbon fibers participating in energy absorption increased as the raster angle increased. Furthermore, the temperature of the extruder was revealed to have a direct correlation to the Charpy impact resistance of the composite, with higher temperatures resulting in increased resistance. At higher temperatures, inter-/intra-layer lamination and thermal bonding are improved, making the composite more resilient to impact. The crystallinity of the printing material also increases with increased temperatures, leading to a significant improvement in Charpy impact strength.[30] This implies that higher temperatures can be beneficial for improving the impact strength of the composite. The Charpy impact strength values were shown to increase as printing speed increases, with only minimal fluctuation between the speeds of 30 and 40 mm/s. The optimum 3D-printing processing parameters and levels were determined to be A5, B3, C2 and D3.

The main effects of the process parameters on the mean response are also studied in addition to the S/N ratio analysis. The average value of each parameter's quality characteristic at various levels is referred to as the mean response. Thus, the average values for each parameter at various levels have been calculated and are displayed in Figure 5B. The mean response analysis also shows that the parameters (A5, B3, C2, and D3) are at the same optimum levels as those found in the S/N ratio analysis. The A5B3C2D3 specimens that are manufactured and tested under the same laboratory conditions are used for validation purposes. The Charpy impact strength was significantly increased when the parameters were optimized. The resulting Charpy impact strength was 10.54 ± 0.76 kJ/m^2, which is almost 1.5 times higher than that of the A2B1C1D2 specimen.

3.4 | Analysis of variance

The ANOVA is a statistical technique that is used to analyze the effect of categorical factors on a response parameter. The technique involves the use of quantities such as degrees of freedom, sum of squares, variance, F-ratio, and percent contribution. Table 4 shows the computed results of the ANOVA with a confidence level of 90%. The p value is used to assess the significance of a parameter. If the p value of a parameter is less than 0.10, it is recognized as being statistically significant. The findings indicate that the infill density (α) is the most influential parameter when it comes to Charpy impact strength of the composites, with it contributing 54% to the total value. Additionally, the raster angle and extruder temperature have been found to contribute 21% and 13%, respectively. However, the effect of printing speed was found to be statistically insignificant within the range of 20–40 mm/s. There are four different processing parameters, three of which are statistically significant. These factors are likely to interact with each other, and an interaction plot can reveal the impact of changing the settings of one experimental parameter on the other parameters. The interactions between the 3D printing parameters are shown in Figure 6. The results of the ANOVA analysis revealed that the printing speed had no significant impact, and thus the printing speed interactions were disregarded for this study. The

TABLE 4 Analysis of variance and GLM of Charpy-impact strength values

Source	DF	Seq SS	Contribution	Adj SS	Adj MS	F-value	p-value
Analysis of variance (ANOVA)							
Raster angle (°)	5	10.701	21.28%	10.701	2.1403	3.04	0.10
Extruder temperature (°C)	2	6.688	13.30%	6.688	3.3440	4.75	0.06
Printing speed (mm/s)	2	1.429	2.84%	1.429	0.7146	1.02	0.42
Infill density (%)	2	27.257	54.19%	27.257	13.6284	19.38	0.002
Error	6	4.220	8.39%	4.220	0.7034		
Total	17	50.296	100.00%				

S	>R-sq	R-sq (adj)	PRESS	R-sq (pred)
General linear model (GLM)				
0.838689	91.61%	76.23%	37.9836	24.48%

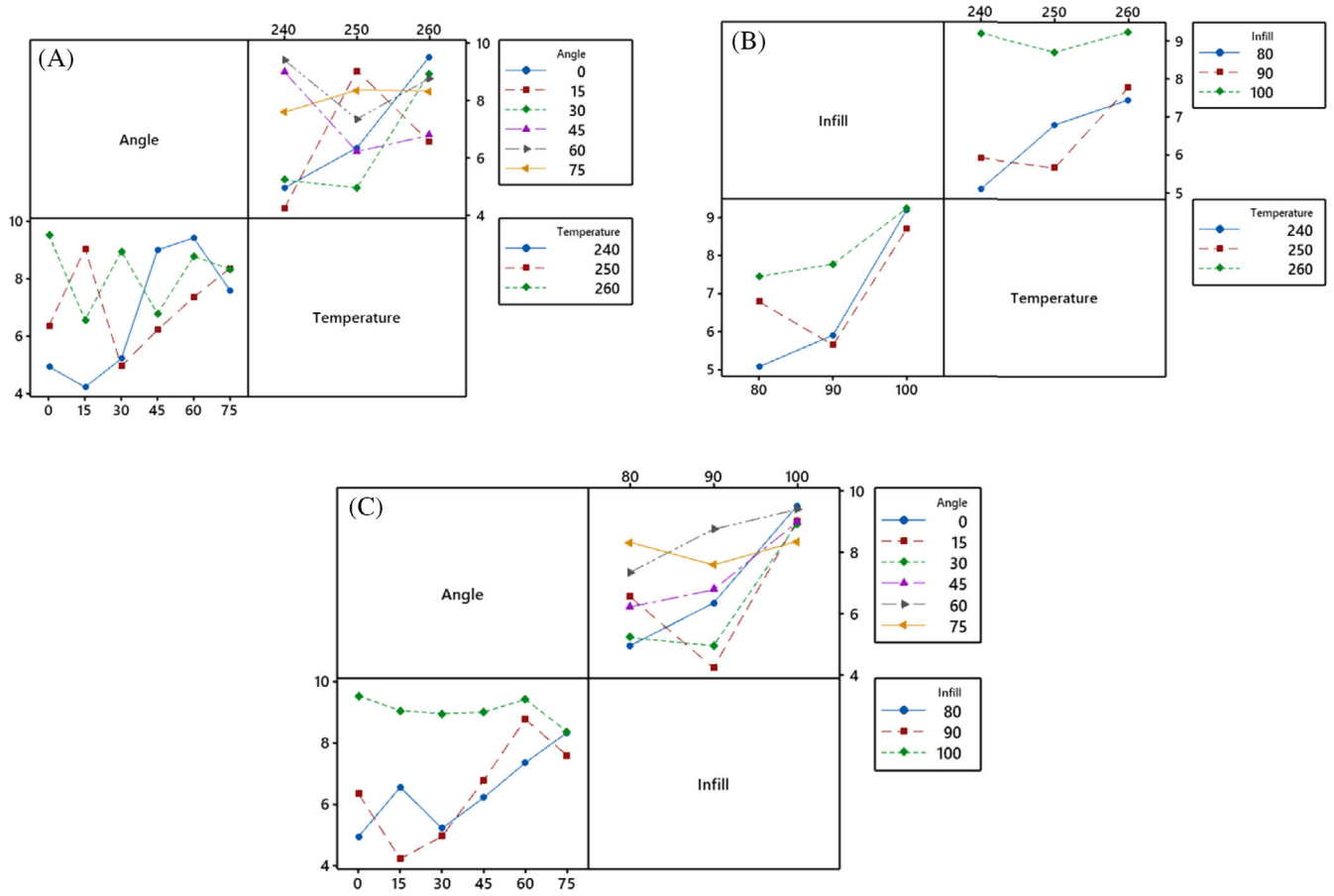

FIGURE 6 Interaction plots from ANOVA (A) raster angle versus temperature, (B) infill density versus temperature and (C) raster angle versus infill density

nonparallel lines in Figure 6A indicated that there was a significant interaction effect between the selected 3D printing parameters and the Charpy impact strength. As can be seen, the effect of raster angle on the Charpy impact strength depends on the level of extruding temperature. The impact resistance of the 3D printed parts was also influenced by infill density and extrusion temperature, as shown in Figure 6B. It was seen that there was also strong interaction between the raster angle and infill density. However, when the infill density reaches 100%, the interactions between these two parameters became insignificant, as shown in Figure 6C.

3.5 | General linear model

A linear relationship between the response and the selected processing parameters can be established by utilizing generalized linear modeling (GLM). The results of the GLM analysis are presented in Table 4, providing a comprehensive overview of the linear relationship between the response and the processing parameters. The coefficient of determination (R^2), which is the strength of the relationship between GLM and the dependent variables on a 0%–100% scale, was determined to be 91.61%. This high R^2 value indicates that it would be easy to predict the Charpy impact strength value by substituting different values of selected process parameters using the Equation (4). The predicted Charpy impact strength of a specimen is the sum of the numerical values of the optimum parameters. For example, if the optimum parameters from Taguchi analysis are raster angle (A5): 60°, temperature (B3): 260 °C, printing speed (C2): 30 mm/s, and infill density (D3): 100%, then the predicted Charpy impact strength of that specimen using GLM would be 11.304 kJ/m^2 (=7.308 + 1.202 + 0.843 + 0.212 + 1.740). The mean absolute percentage error (MAPE) between the experimental and predicted Charpy impact strength values for the A5B3C2D3 specimen was calculated to be 7.21%.

$$\begin{aligned}\text{Charpy impact strength}\left(\text{kJ/m}^2\right) &= 7.308 - 0.371 \times (\text{A1}) - 0.699 \times (\text{A2}) - 0.937 \times (\text{A3}) \\ &+ 0.02 \times (\text{A4}) + 1.202 \times (\text{A5}) + 0.786 \times (\text{A6}) - 0.579 \\ &\times (\text{B1}) - 0.264 \times (\text{B2}) + 0.843 \times (\text{B3}) - 0.398 \times (\text{C1}) \\ &+ 0.212 \times (\text{C2}) + 0.186 \times (\text{C3}) - 0.874 \times (\text{D1}) - 0.867 \\ &\times (\text{D2}) + 1.740 \times (\text{D3}) \end{aligned} \quad (4)$$

The experimental and predicted values of Charpy impact strength for all 18 groups are shown in Figure 7B. The experimental and predicted points for all 18 groups in the graph were quite close to each other, with a mean absolute percentage error (MAPE) of 5.94%. This indicates that the proposed equation is successful in accurately predicting the Charpy impact strength of CF/PA composites.

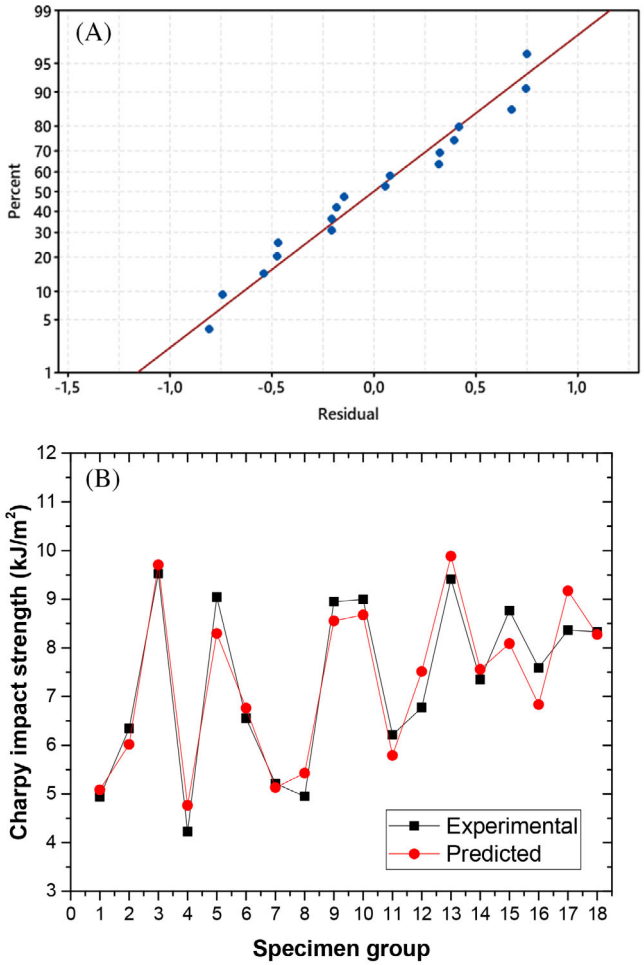

FIGURE 7 (A) Normal probability plot for GLM and (B) experimental versus the predicted values of Charpy impact strength

3.6 | Regression analysis

The regression analysis is a statistical method used to analyze the relationship between independent and dependent variables. In this analysis, a function is sought that can adequately explain the change of the target parameter based on the input factors, while having the minimum possible error of prediction.[31] In this study, the mathematical expression for the estimate of the Charpy impact strength values of the composites is determined using quadratic regression analysis. The estimated quadratic regression line on the experimental Charpy impact strength vs. the predicted values is shown in Figure 8. The mathematical expression for the estimate of the Charpy impact strength values of composites was determined using quadratic regression analysis. The estimated quadratic regression line on the experimental Charpy impact strength vs the predicted values is shown in Figure 8. R-squared was determined as 93.2%, which means that 93.2% of the experimental data should fall within the regression line. The high R-squared value (0.932) and adjusted R-squared value (0.923) are nearly comparable, indicating that the regression model well predicted the response of the experimental data.

3.7 | Fracture surface analysis

The surface morphologies of the A2B1C1D2 (DOE-4) and the Taguchi specimen produced with the optimum 3D printing parameters (A5B3C2D3) were examined with a Carl Zeiss Leo G34-Supra 35VP scanning electron microscope (Zeiss LSM5 Pascal, Oberkochen, Germany). The samples were sputter-coated with gold and viewed under an accelerating voltage of 3 kV. Since the most important parameters and their contributions have been identified from the ANOVA analysis, the SEM interpretations will focus on the effects of these critical 3D-printing parameters on the microstructural damage state of the CF/PA composites. The SEM images in Figure 9A–C illustrate the fracture surfaces of the A2B1C1D2 (DOE-4) specimen, which had the lowest Charpy impact strength. At lower magnifications (Figure 9B), the layers did not adhere well due to the low printing temperature (240°C). The formation of voids was observed which can be attributed to the lack of a robust fiber-matrix interface and the separate motion of the fibers and matrix during extrusion. The differences between the coefficient of thermal expansion of the fiber and matrix are a major factor in the formation of voids. Moreover, the addition of short carbon fibers affects the rheology of the polymer, resulting in an increased viscosity of the polymer composite melt and a higher likelihood of voids

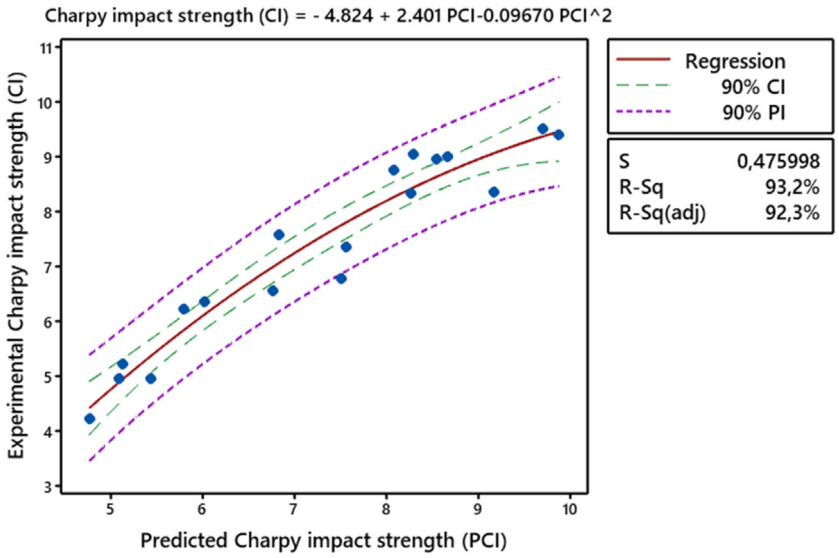

FIGURE 8 The predicted Charpy impact strength versus experimental Charpy impact strength fitted with the quadratic regression line

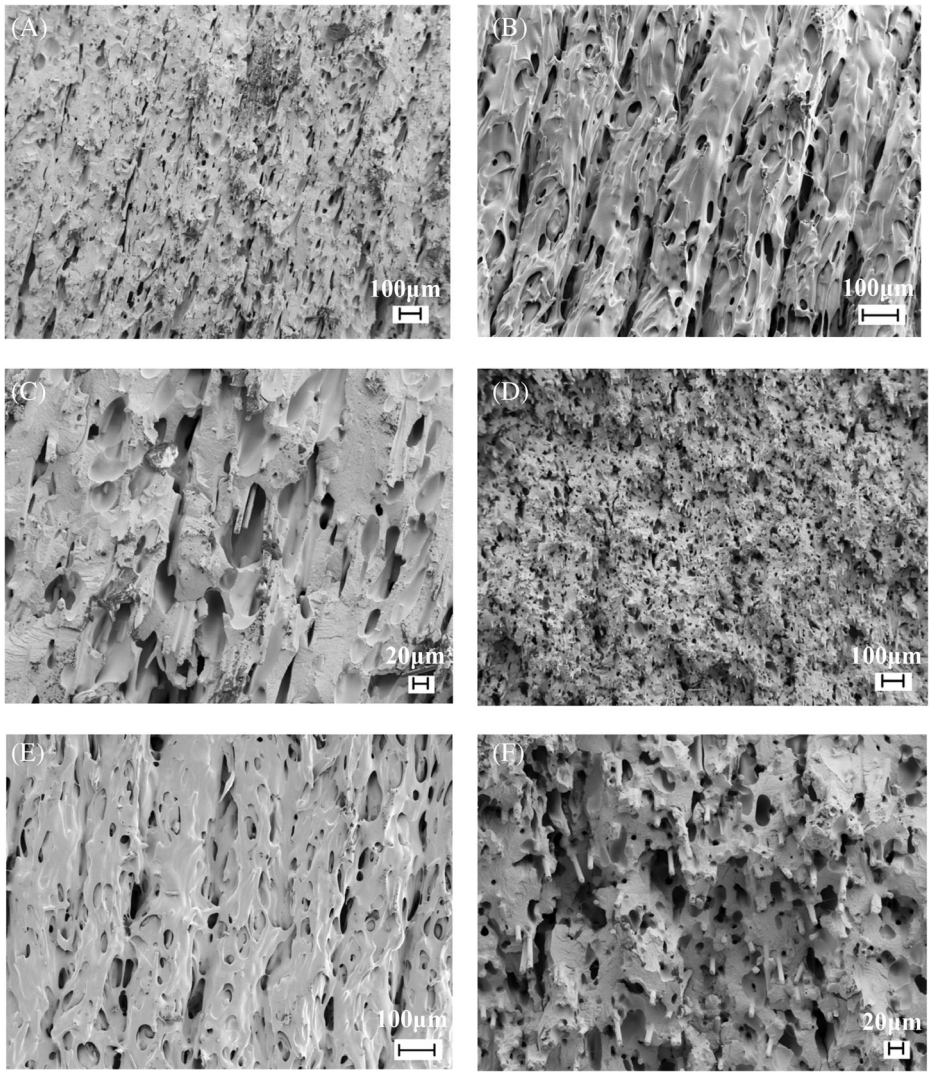

FIGURE 9 SEM images of (A–C) the A2B1C1D2 specimen (DOE-4) and (D–F) the A5B3C2D3 specimen produced with the optimized 3D-printing parameters

appearing.[32–34] A small amount of carbon fibers, which were pulled out from the matrix, and some fractured carbon fibers can be seen in Figure 9C.

The SEM images in Figure 9D–F show the fracture surfaces of the Taguchi specimen printed with the optimum printing parameters (A5B3C2D3). Figure 9E shows that the gap between layers decreased, and the number of voids decreased due to the higher printing temperature (260°C) compared to the A2B1C1D2 specimen. This is because the higher printing temperature increases the melt viscosity of the polymer, resulting in a stronger interfacial bond between adjacent layers. As the temperature increases, the adhesion of the newly printed material to the extruded material is enhanced, resulting in a greater bond width between the extruded raster patterns. This increased bond width increases the impact resistance of the material. Moreover, higher printing temperatures provide adequate energy to melt the material and permit additional time for PA crystallization, which is demonstrated to be a major factor influencing the mechanical properties of 3D printed materials. Another reason is that the shear stresses that are generated during 3D printing induce the alignment of carbon fibers in composites along the extrusion direction.[35,36] Figure 9D,F demonstrate numerous voids (or darker dots) that resemble the cross sections of carbon fiber reinforcement. These voids were formed due to the carbon fiber pullouts that occurred during specimen failure, which in turn enhanced the energy absorption properties of the composites and increased their impact toughness. The energy-absorbing mechanism that facilitated this was the pulling of carbon fibers from their sockets within the polyamide matrix during crack propagation. This was enabled after the interfacial debonding and fiber fracture outside of the crack plane had already taken place. The fractured carbon fibers reveals that the stress from the thermoplastic matrix was efficiently conveyed to the carbon fibers, thus resulting in a higher impact strength. Upon comparison of A5B3C2D3 specimen with A2B1C1D2 specimen, the alteration of infill density from 90% to 100% resulted in an increase of the amount of thermoplastic polymer and carbon fiber material within the test specimen (illustrated in Figure 9B,E). This, in turn, lead to more carbon fibers participating in the pullout toughening mechanism. The rasters demonstrated an increased inclination in the direction of loading, thus augmenting the impact resistance of the specimens.

3.8 | Infrared thermography

Thermography is a popular non-destructive technique for structures reliability due to its easy use and rapid results. In this study, lock-in thermography process on the impact test specimens was performed to evaluate the void content, heat loss, and damage status of impact test specimens. The experimental setup for IRT testing of the specimens is shown in Figure 10A. A FLIR X6580 SC thermal imaging camera equipped with 25 mm lens and Indium antimonide photon detector was used in the analysis. Edevis VISIT V 302/700 S control unit is utilized in the system, which connected to the IR camera for thermal scanning of the specimens, while Hedler® light system (3× H25s lamps, max 2.5 kW) was used to perform the thermal stimulation on the specimen surfaces. A heating cycles with a frequency of 0.02 Hz was performed with a sinusoidal signal with the light system. The captured thermal data (sampling rate of 30 Hz) were processed with DisplayImg 6 software.

The thermography images of the A2B1C1D2 and A5B3C2D3 specimens in Figure 10B revealed that the A5B3C2D3 specimen was in a significantly more structurally intact than the A2B1C2D3 specimen, signifying better adhesion between the built-up layers and thus an improved impact toughness. Moreover, the thermography images also show a decreased heat loss from the lower part of the A5B3C2D3 specimen, indicating a lower void content. This was further corroborated by the SEM analysis.

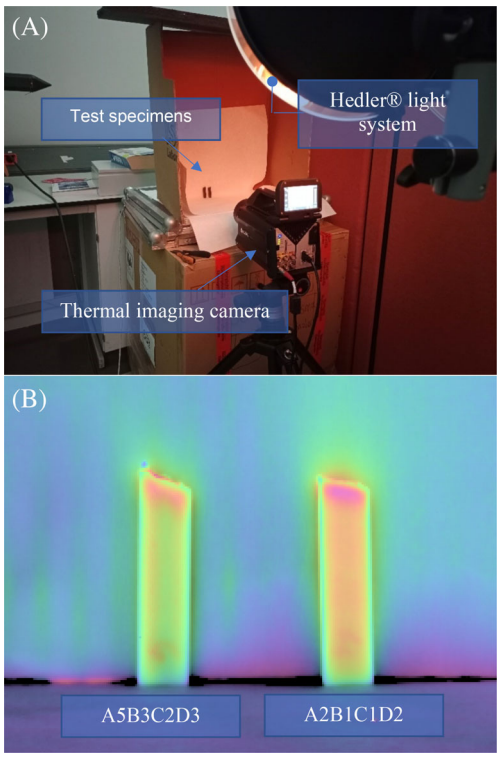

FIGURE 10 (A) IRT test setup. (B) The thermography images of A5B3C2D3 (optimized) and A2B1C1D2 impact specimens

4 | POTENTIAL APPLICATIONS

Polyamides reinforced with short carbon fibers are rapidly gaining traction in various industries, due to their cost-effectiveness, straightforward handling, and satisfactory mechanical performance. The aerospace industry has employed the potential of short-fiber reinforced thermoplastics in various components of the A340-600 and A350 XWB, and V-22 tilt-rotor aircraft.[37] These components are typically manufactured through extrusion compounding and injection molding processes. To determine potential uses for 3D-printed CF/PA parts, a comparison of the mechanical performance between CF/PA composites produced by 3D printing and those produced through injection molding/extrusion should be conducted using the same quantity of carbon fibers. It is essential to make this comparison to reach a decisive conclusion regarding potential applications for 3D-printed CF/PA parts.

Toro et al.[5] demonstrated that the tensile strength, yield strength and elastic modulus of CF/PA parts produced using FDM were lower than those made with injection molding, though the difference stayed below 21% in all experiments. Through careful optimization of 3D printing process parameters, it is possible to reduce the decline in tensile performance to an acceptable level. Additionally, the results of the compression test showed a slight difference of approximately 4% between 3D-printed CF/PA parts and injection molded parts. Furthermore, stiffness values for 3D-printed CF/PA specimens were found to be higher than those for injection molded CF/PA parts. Sang et al.[38] reported that the Charpy impact strength of CF/PA parts (carbon fiber content: 20 wt%) produced by injection molding was 6.4 kJ/m^2. Molnar et al.[39] showed that the Charpy impact strength of CF/PA injection-molded materials changed according to the amount of carbon fiber present, ranging from 6 to 12 kJ/m^2 for samples with 0 to 14 vol% of the carbon fiber. Our findings demonstrated that the ideal 3D-printing parameters can result in CF/PA components with a Charpy impact strength of 10.5 kJ/m^2. This implies that components produced by FDM may be able to substitute for structures traditionally created via injection molding and extrusion when the processing parameters are optimized. In situations where small batches of intricate parts need to be produced, 3D printing is a more desirable solution due to its lack of necessity for substantial capital investments, making it a more viable alternative than other capital-intensive processes.

5 | CONCLUSION

In this study, the Charpy impact strength of specimens produced by a 3D printer composed of CF/PA was evaluated both experimentally and statistically while taking into consideration four different parameters of FDM, namely, raster angle, extruder temperature, printing speed, and infill density. The Taguchi L18 orthogonal array was implemented to create the experimental plan. Signal to Noise (S/N) ratios and Analysis of Variance (ANOVA) were employed to discover the best levels and interactions of the parameters. Scanning electron microscopy (SEM) and infrared thermography (IRT) techniques were applied to assess the microstructural and damage state of the composite specimens. The results demonstrate that the optimal 3D printing parameters are infill density (100%), raster angle (60°), extruder temperature (260°C), infill density (100%), and printing speed (30 mm/s). The analysis of variance (ANOVA) results indicate that infill density, raster angle, and extruder temperature were the only parameters that were statistically significant. The best combination of printing parameters yielded a Charpy impact strength of 10.54 kJ/m^2, representing an increase of 149.5% compared to the least successful case. This study demonstrated that the Taguchi method is a viable option for optimizing the Charpy impact strength of 3D-printed CF/PA composites.

ACKNOWLEDGMENTS

The authors gratefully acknowledge the financial support of The Scientific and Technological Research Council of Turkey, TUBITAK (1002-Short Term R&D Funding Program, Grant number: 219M076).

CONFLICT OF INTEREST STATEMENT

The authors declare that there is no conflict of interest.

DATA AVAILABILITY STATEMENT

The data that support the findings of this study are available from the corresponding authors upon reasonable request.

ORCID

Bertan Beylergil https://orcid.org/0000-0002-3204-6746
Mehmet Yildiz https://orcid.org/0000-0003-1626-5858

REFERENCES

[1] M. Hikmat, S. Rostam, Y. M. Ahmed, *Results Eng.* **2021**, *11*, 100264.
[2] D. Popescu, A. Zapciu, C. Amza, F. Baciu, R. Marinescu, *Polym. Test.* **2018**, *69*, 157.
[3] J. R. C. Dizon, A. H. Espera, Q. Chen, R. C. Advincula, *Addit. Manuf.* **2018**, *20*, 44.
[4] M. Chapiro, *Reinf. Plast.* **2016**, *60*(6), 372.
[5] E. V. de Toro, J. C. Sobrino, A. M. Martínez, V. M. Eguía, *Procedia Manuf.* **2019**, *41*, 731.
[6] V. Mahesh, *Polym. Compos.* **2021**, *42*(10), 5021.
[7] X. Jing, Y. Duan, F. Xie, C. Zhang, S. Chen, *Polym. Compos.* **2022**, 1. DOI: 10.1002/pc.27187

[8] C. A. Murphy, M. N. Collins, *Polym. Compos.* **2018**, *39*, 1311.
[9] D. Mohan, A. N. Bakir, M. S. Sajab, et al., *Polym. Compos.* **2021**, *42*, 2408.
[10] J. Bustillos, D. Montero-Zambrano, A. Loganathan, B. Boesl, A. Agarwal, *Polym. Compos.* **2019**, *40*, 379.
[11] V. Mahesh, A. S. Joseph, V. Mahesh, D. Harursampath, C. Vn, *Polym. Compos.* **2021**, *42*, 2380.
[12] J. Bustillos, D. Montero, P. Nautiyal, A. Loganathan, B. Boesl, A. Agarwal, *Polym. Compos.* **2018**, *2018*(39), 3877.
[13] A. K. Sood, R. K. Ohdar, S. S. Mahapatra, *Mater. Des.* **2010**, *31*, 287.
[14] D.-A. Türk, F. Brenni, M. Zogg, M. Meboldt, *Mater. Des.* **2017**, *118*, 256.
[15] J. M. Chacón, M. A. Caminero, E. García-Plazai, P. J. Núñez, *Mater. Des.* **2017**, *124*, 143.
[16] S. Wang, Y. Ma, Z. Deng, S. Zhang, J. Cai, *Polym. Test.* **2020**, *86*, 106483.
[17] S. Raut, V. S. Jatti, N. K. Khedkar, T. P. Singh, *Proc. Mater. Sci.* **2014**, *6*, 1625.
[18] H. K. Sezer, O. Eren, H. R. Börklü, V. Özdemir, *J. Fac. Eng. Archit. Gazi Univ.* **2019**, *34*(2), 663.
[19] F. Ning, W. Cong, Y. Hu, H. Wang, *J. Compos. Mater.* **2016**, *51*(4), 451.
[20] X. Peng, M. Zhang, Z. Guo, L. Sang, W. Hou, *Compos. Commun.* **2022**, *22*, 100478.
[21] V. Shanmugam, M. V. Pavan, K. Babu, B. Karnan, *Polym. Compos.* **2021**, *42*(11), 5656.
[22] S. Raja, A. Verma, S. M. Rangappa, S. Siengchin, *Polym. Compos.* **2022**, *43*(8), 5523.
[23] A. Shabani, A. Babaei, A. R. Zanjanijam, M. Ramezani, M. H. Abdolrasouli, *Polym. Compos.* **2019**, *40*(12), 4753.
[24] X. Liu, M. Zhang, S. Li, L. Si, J. Peng, Y. Hu, *J. Adv. Manuf. Technol.* **2016**, *89*(5), 2387.
[25] L. Sang, C. Wang, Y. Wang, Z. Wei, *RSC Adv.* **2017**, *7*, 43334.
[26] X. Wang, H. Yang, L. Song, Y. Hu, W. Xing, H. Lu, *Compos Sci Technol* **2011**, *72*(1), 1.
[27] A. A. Ansari, M. Kamil, *Int. J. Lightweight Mater. Manuf.* **2022**, *5*, 369.
[28] M. Dhanalakshmi, J. P. Jog, *Express Polym Lett.* **2008**, *2*(8), 540.
[29] J. O. Fernandez, G. M. Swallowe, S. F. Lee, *J. Appl. Polym. Sci.* **2000**, *80*, 2031.
[30] B. M. Tymrak, M. Kreiger, J. M. Pearce, *Mater. Des.* **2014**, *58*, 242.
[31] R. Gholami, N. Fakhari, in *Handbook of Neural Computation* (Eds: P. Samui, S. Sekhar, V. E. Balas), Academic Press, Cambridge **2017**, p. 515.
[32] D. Yang, H. Zhang, J. Wu, E. D. McCarthy, *Addit. Manuf.* **2021**, *37*, 101686.
[33] H. L. Tekinalp, V. Kunc, G. M. Velez-Garcia, C. E. Duty, L. J. Love, A. K. Naskar, C. A. Blue, S. Ozcan, *Compos. Sci. Technol.* **2014**, *105*, 144.
[34] S. Yu, Y. H. Hwang, J. Y. Hwang, S. H. Hong, *Compos. Sci. Technol.* **2019**, *175*, 18.
[35] D. Syrlybayev, B. Zharylkassyn, A. Seisekulova, M. Akhmetov, A. Perveen, D. Talamona, *Polymer* **2021**, *13*(10), 1587.
[36] A. Lee, M. Wynn, L. Quigley, M. Salviato, N. Zobeiry, *Adv. Ind. Manuf. Eng.* **2022**, *4*, 100085.
[37] E. Kurkin, M. Spirina, O. U. E. Barcenas, E. Kurkina, *Polymer* **2022**, *14*, 1781.
[38] L. Sang, C. Wang, Y. Wang, W. Hou, *Compos. Part B-Eng.* **2018**, *153*, 306.
[39] S. Molnár, S. Rosenberger, J. Gulyás, B. Pukánszky, *J. Macromol. Sci. Phys.* **1999**, *38*, 721.

SUPPORTING INFORMATION

Additional supporting information can be found online in the Supporting Information section at the end of this article.

How to cite this article: B. Beylergil, A. Al-Nadhari, M. Yildiz, *Polym. Compos.* **2023**, *44*(5), 2846. https://doi.org/10.1002/pc.27285